Involvement of RNase J in CRISPR RNA maturation and degradosome formation in cyanobacteria

Raphael Bilger[1], Friedel Drepper[2], Bettina Knapp[2], Tanja Berndt[1], Helena Landerer[1], Harald Putzer[3], Pitter Huesgen[2,4] and Wolfgang R. Hess[1,*]

[1]University of Freiburg, Faculty of Biology, Genetics and Experimental Bioinformatics, Schänzlestr. 1, D-79104 Freiburg, Germany

[2]University of Freiburg, Faculty of Biology, Biochemistry and Functional Proteomics, Schänzlestr. 1, D-79104 Freiburg, Germany …

[3]Expression Génétique Microbienne (EGM), CNRS, Université Paris Cité, Institut de Biologie Physico-Chimique, F- 75005 Paris, France

[4]University of Freiburg, CIBSS Centre for Integrative Biological Signalling Studies, D-79104 Freiburg, Germany

*Corresponding authors: Wolfgang R. Hess; Phone: +49-761-2032796; E-mail: wolfgang.hess@biologie.uni-freiburg.de

Keywords: CRISPR-Cas systems, cyanobacteria, degradosome, gene expression regulation, ribonuclease J, RNA structure, RNA:RNA interaction

Abstract

Many bacteria and archaea use CRISPR-Cas systems, which provide RNA-based, adaptive, and inheritable immune defenses against invading viruses and other foreign genetic elements. The proper processing of CRISPR guide RNAs (crRNAs) is a crucial step in the maturation of the defense complexes and is frequently performed by specialized ribonucleases encoded by *cas* genes. However, some systems employ enzymes associated with degradosome or housekeeping functions, such as RNase III or the endoribonuclease RNase E. Here, the endo- and 5´-exoribonuclease RNase J was identified as additional enzyme involved in crRNA maturation, acting jointly with RNase E in the crRNA maturation of a type III-Bv CRISPR-Cas system, and possibly together with a further RNase. Co-IP experiments revealed a small set of proteins that were co-enriched with RNase J, among them PNPase. Despite a measured, strong 3' exonucleolytic activity of the recombinant enzyme, PNPase was not confirmed to contribute to crRNA maturation. However, the co-IP results indicate that PNPase is a component of the cyanobacterial degradosome that can recruit either RNase E or RNase J, together with additional enriched proteins.

Introduction

Bacteria are exposed to many environmental changes that require rapid acclimation responses, including the regulation of gene expression. One mechanism is the post-transcriptional regulation of mRNA decay involving the activity of one of the major ribonucleases (RNases), RNase E/G, RNase Y, and/or RNase J. In all bacteria, at least one homolog of these RNases can be found (Laalami, Zig and Putzer 2014; Aït-Bara and Carpousis 2015).

RNases are often the scaffold for an mRNA degradation machinery, the degradosome. In *E. coli*, RNase E possesses binding domains in its C-terminal region to recruit the exoribonuclease polyribonucleotide nucleotidyltransferase (PNPase), the RNA helicase RhlB and the glycolytic enzyme enolase (Vanzo *et al.* 1998). In the gram-positive bacterium *B. subtilis*, the degradosome complex is assembled around RNase Y, which, similarly to the *E.coli* degradosome, interacts with PNPase, the helicase CshA and enzymes involved in glycolysis (Commichau *et al.* 2009; Lehnik-Habrink *et al.* 2010; Newman *et al.* 2012).

An RNase E-based RNA degradosome exists also in cyanobacteria (Zhang, Hess and Zhang 2022). It was first shown in the filamentous cyanobacterium *Nostoc* (*Anabaena*) sp. PCC 7120 that the noncatalytic region of RNase E recruited PNPase, and that the two proteins interact through a widely conserved nonapeptide within the RNase E C-terminal region (subregion C435) (Zhang *et al.* 2014). Later, the 3' exoribonuclease RNase II was found to be another RNase E-associated ribonuclease in this organism (Zhou *et al.* 2020), and there is strong evidence for further additional interacting proteins, such as the RNA helicase CrhB, enolase (Yan *et al.* 2020), and the

conserved protein RebA (Liu *et al.* 2024). RebA is an inhibitor of RNase E catalytic activity and is universally conserved in cyanobacteria (Liu *et al.* 2024).

Besides mRNA degradation, the degradosome enzymes play important roles in other biological processes, such as in the control of translation (Redko *et al.* 2013) or the maturation of CRISPR-related transcripts (crRNAs) (Behler *et al.* 2018). The type III-A CRISPR/Cas system of *Staphylococcus epidermidis* relies on the degradosome associated PNPase and RNase J2 to promote crRNA maturation and for efficient clearance of phage-derived nucleic acids (Chou-Zheng and Hatoum-Aslan 2019).

In the cyanobacterial model *Synechocystis* sp. PCC 6803 (hereafter *Synechocystis*), three distinct CRISPR/Cas systems were described. These are a type I-D (CRISPR1), a type III-Dv (CRISPR2), and a III-Bv (CRISPR3) system, which are highly expressed under a variety of conditions and active in interference assays (Scholz *et al.* 2013, 2019; Kieper *et al.* 2018; McBride *et al.* 2020; Bilger *et al.* 2024; Schwartz *et al.* 2024). While the CRISPR1 and CRISPR2 systems depend on Cas6 riboendonucleases for the maturation of crRNAs (Scholz *et al.* 2013; Reimann *et al.* 2017), no such enzyme is affiliated with the CRISPR3 system. Instead, RNase E processes crRNAs in this system by a single cleavage within the repeats, directly generating the 13 and 14 nt long 5’ repeat handles (Behler *et al.* 2018). However, the sequences between the spacer ends and the 5’ handle of the next following crRNA disappear and also do not accumulate as individual fragments. These observations and the accumulation of mature crRNAs exclusively 48 and 42 nt in length suggested the involvement of at least one additional ribonuclease in the maturation of CRISPR3-derived crRNAs (Scholz *et al.* 2013; Behler *et al.* 2018).

In addition to RNase E (*slr1129*), RNase J (*slr0551*) is present in *Synechocystis*, a combination that is conserved in cyanobacteria (Laalami and Putzer 2011). RNase E has been analyzed in more depth than RNase J, but it is clear that both enzymes target a wide range of transcripts (Cavaiuolo *et al.* 2020; Hoffmann *et al.* 2021, 2024). Neither the gene encoding RNase E nor the gene for RNase J can be deleted in *Synechocystis* indicating their essentiality. However, *Synechocystis* contains multiple chromosome copies (Zerulla, Ludt and Soppa 2016), making partial gene deletions possible. Analysis of such a partial *rnj* deletion (strain δ*rnj*) indicated that the maturation of crRNAs from the CRISPR3 system could involve RNase J (Cavaiuolo *et al.* 2020).

RNase J was first discovered in *Bacillus subtilis* (Even *et al.* 2005), but is wide-spread also in other bacteria, in many archaea (Hasenöhrl, Konrat and Bläsi 2011; Levy *et al.* 2011; Zheng *et al.* 2017), and also present in plant and algal chloroplasts (Chen, Zou and Zhao 2015; Liponska *et al.* 2018; Hotto, Stern and Schuster 2020). RNase J belongs to the β-CASP protein family within the superfamily of metallo-β-lactamase fold proteins (Callebaut *et al.* 2002), with two beta lactamase domains separated by a β-CASP domain (Condon and Gilet 2011). The enzyme possesses an endonuclease and a unique 5'-3' exonuclease activity (Mathy *et al.* 2007), the latter previously thought to be absent in prokaryotes (Alifano, Bruni and Carlomagno 1994; Deana and Belasco 2005). Despite these insights, RNase J is still less well investigated in comparison to RNase E (Ehretsmann, Carpousis and Krisch 1992; Mackie 2013; Zhang *et al.* 2014; Chao *et al.* 2017; Hoffmann *et al.* 2021, 2024; Liu *et al.* 2024), or RNase Y (Shahbabian *et al.* 2009; Lehnik-Habrink *et al.* 2011; Marincola *et al.* 2012; Scornet *et al.* 2024).

Here, we investigated if RNase J is involved in the maturation of pre-crRNA in *Synechocystis* and identified putative cleavage sites. Through co-immunoprecipitation

(co-IP) coupled with mass spectrometry we identified RNase J interaction partners, pointing at possible further partners in an RNase J-based RNA degradosome in *Synechocystis.*

Methods

Strains and cultivation

Synechocystis cultures were grown at 30°C in 50 mL copper-depleted BG11 medium (Rippka *et al.* 1979) supplemented with 20 mM TES (N-[Tris-(hydroxymethyl)-methyl]-2-aminoethane sulfonic acid) under continuous illumination with white light at 30 – 50 µmol photons m^{-2} s^{-1} and constant shaking. The cultures were supplied with appropriate antibiotics, namely kanamycin (50 µg/mL) and gentamicin (2 µg/mL) for *Synechocystis* strains carrying pVZ322 (Zinchenko *et al.* 1999) constructs, and kanamycin (100 µg/mL) and spectinomycin (200 µg/mL) for the strains carrying the spectinomycin resistance cassette and a pVZ322 vector. For co-IP assays, four biological replicates of strains overexpressing N- or C-terminally tagged RNase J and GFP controls were cultivated in the CellDEG HD cultivator system (CellDEG GmbH) in 100 mL of fresh water organism (FWO) medium at a starting OD_{750} of 0.9 – 1.0. Kanamycin and gentamicin were added as described (Migur *et al.* 2021). RNase J or GFP expression was induced with 2 µM of Cu^{2+} or 6 mg/mL of L-rhamnose, according to the expression system, for 24 h before harvesting (final OD_{750} of approximately 25 – 30). An equivalent of 1000 OD of cells were collected by centrifugation (3,200 × g, 10 min, at room temperature). Pellets were stored at -70°C until further processing.

Construction of RNase J expression vectors

We constructed two different systems for the expression of 3×FLAG-tagged RNase J. First, we constructed the pVZ322-P_{petE}-*slr0551* vector with and without a C-terminal 3×FLAG tag. The *slr0551* native gene and the *petE* gene promoters were amplified from *Synechocystis* genomic DNA using primer pairs RB1/ RB2 and RB3/RB4, respectively. The PCR products were separated on 0.8% agarose gels, visualized with ethidium bromide and correctly-sized fragments were excised and purified with the NucleoSpin Gel and PCR Clean-up kit (Machery-Nagel GmbH), according to manufacturer's instructions. Then, the fragments were ligated by AQUA cloning (Beyer *et al.* 2015) into pUC19 reverse-amplified by PCR with primers RB5/ RB6 and transformed into chemically competent *E. coli* DH5α cells (NEB). After confirming correct insert sequences, P_{petE}-*slr0551* was amplified using primers RB7/ RB8, or primers RB9/ RB10 to generate fragments for the inducible RNase J expression with and without a C-terminally 3×FLAG tag. The fragments were ligated into *Pst*I/*Xba*I-digested pVZ322 via AQUA cloning. The final pVZ322 constructs were introduced into the *Synechocystis* wild type, WT-Spc and δ*rnj* (Cavaiuolo *et al.* 2020) strains by tri-parental mating (Scholz *et al.* 2013). Constructs were verified via PCR and sequencing.

To construct plasmid pVZ322-P_{rha}-3×FLAG-*slr0551* for the expression of RNase J with an N-terminal 3×FLAG tag under the control of an rhamnose-inducible promoter (Kelly *et al.* 2018, 2019), primers RB11/ RB12 were used to amplify a 3×*flag-slr0551* fragment. In parallel, the backbone was reverse-amplified from plasmid pUC19P_{rha}YFP3×FLAG (Hemm *et al.* 2024) using primer pair RB13/ RB14 . After gel separation and excision, the two amplicons were treated with FastDigest *Dpn*I (Thermo Fisher Scientific) to eliminate template DNA. The construct was assembled

via AQUA cloning (Beyer *et al.* 2015) by transformation into DH5α chemical competent *E. coli* cells (NEB). Correct insertion of the *slr0551* fragment was checked by colony PCR with primer pair RB15/ RB16 using One*Taq* polymerase (NEB) and positive clones were sequenced by IDT (Integrated DNA Technologies, Inc). Correct constructs were selected for PCR with primer pair RB15/ RB16 using PCRBio HiFi polymerase (PCR Biosystems Ltd.) and cloned into *Xmn*I-digested pVZ322s (pVZ322 lacking the kanamycin cassette (Kaltenbrunner *et al.* 2023)) by AQUA cloning. The verified construct was then introduced in *Synechocystis* wild type via tri-parental mating (Scholz *et al.* 2013). Correct clones were identified by PCR and verified by sequencing. Primers used in this work are listed in **Supplementary Table S1**.

RNA isolation

Synechocystis wild type, the strain with spectinomycin cassette integrated into a neutral site (in the *ssl0452-slr0271* intergenic region, strain WT-Spc (Cavaiuolo *et al.* 2020)), and δ*rnj* strains with and without pVZ322 constructs for RNase J expression were cultivated in copper depleted BG11 with appropriate antibiotics. When the cultures reached an OD_{750} of approximately 0.5, they were induced with 2 µM $CuSO_4$ and collected by vacuum filtration on hydrophilic polyethersulfone filters (Pall Supor®-800, 0.8 µm) at time point 0 (before induction), and 24 and 48 h thereafter. The filter was transferred to a tube containing 1 mL of PGTX (39.6 g phenol, 6.9 g glycerol, 0.1 g 8-hydroxyquinoline, 0.58 g EDTA, 0.8 g sodium acetate, 9.5 g guanidine thiocyanate, 4.6 g guanidine hydrochloride) (Pinto *et al.* 2009), snap frozen in liquid nitrogen and stored at - 80°C. For the RNA extraction, the samples were incubated for 15 min at 65°C, 1 mL of chloroform/isoamyl alcohol (IAA) (24:1) was added and the samples

were incubated for 10 min at room temperature. Phase separation was performed by centrifugation for 5 min at 3,270 × g at room temperature. The upper aqueous phase was transferred to a new tube, mixed with one volume of chloroform/IAA (24:1) and centrifuged again. The aqueous phase was transferred to a new tube, mixed with one volume of isopropanol and precipitated overnight at -20°C. The precipitated RNA was pelleted by centrifugation (13,000 × g, 30 min, 4°C). The pellet was washed with 700 µL of 70% ethanol (13,000 × g, 10 min, 4°C), air-dried and resuspended in 20 – 40 µL of nuclease-free water. RNA concentration was determined using a spectrophotometer (NanoDrop ND-1000, Peqlab). The RNA quality was assessed by loading 10 µg of RNA on an 8 M urea, 10% polyacrylamide (PAA)-Tris-Borate-EDTA (TBE) gel.

Primer extension assay

Primer extension was performed as described previously (Behler *et al.* 2018) using the primers RB17 and RB18 (called PrimerExt_Ladder_fwd and PrimerExt_S3_rev in Behler *et al.* (2018)) to target the same region in the CRISPR3 pre-crRNA transcript, and using RNA from *Synechocystis* WT-Spc or δ*rnj* strains, carrying different pVZ322 constructs. The cells were harvest 24 h post-induction and RNA was isolated as described above.

RNase J co-IP and proteomic sample preparation:

Cell pellets from CellDEG cultures were resuspended in 1.5 mL FLAG buffer (50 mM Hepes-NaOH pH 7.5 mM $MgCl_2$, 25 mM $CaCl_2$, 150 mM NaCL, 10% glycerol, 0.1%

Tween-20 and cOmplete Protease inhibitor (Roche)) and split in three screw-cap tubes containing 250 µL glass beads (Ø 0.1-0.25 mm, Retsch). The cells were lysed using a prechilled Precellys homogenizer (Bertin Technologies). To remove cell debris and glass beads, the samples were centrifuged at 13,000 × g for 30 min at 4°C. The supernatant (soluble crude extract) was incubated with 100 µL of packed anti-FLAG® M2 magnetic beads (Sigma Aldrich), for 2 hours at 4°C under gentle rotation. The beads were washed 6 times with 2 mL of FLAG-buffer using DynaMag™-2 magnetic rack (Thermo Fisher). The attached proteins were eluted with 250 µL TBS containing 0.4 mg/mL FLAG peptide as competitor. The samples were incubated for 30 min at 4°C under gentle rotation. The supernatant was taken as elution fraction.

For MS analysis, 10 µg of protein per sample was prepared by adding 1% SDS and 5 mM DTT, followed by an incubation at 60°C for 30 min with shaking at 1,000 rpm. in a ThermoMixer® (Eppendorf). Reduced disulfides were alkylated by adding 0.1 vol of 2-chloroacetamide (200 mM) and incubation for 15 min at 37°C and shaking. The alkylation reaction was quenched by adding 5 mM of DTT. The protein clean-up and digestion was performed following the SP3 protocol (Hughes *et al.* 2019). To each sample, 100 µg of a 1:1 mixture of Sera-Mag SpeedBeads suspension (prepared to a 50 µg/µL, GE Healthcare®, cat. No. 45152105050250 and 65152105050250) was added. To induce binding of the proteins to the beads, 4 vol of 100% ethanol were added and incubated in a ThermoMixer® at 24°C for 5 min at 1,000 rpm. Tubes were placed in a magnetic rack and the beads were washed 3 times with 180 µL of 80% ethanol. Beads were resuspended in 75 µl of 100 mM ammonium bicarbonate, pH 8 containing 0.24 µg of sequencing grade, modified trypsin (Promega), sonicated for 30 s in a water bath to disaggregate the beads and incubated for 18 h at 37°C in a ThermoMixer® at 1,000 rpm. After digestion, the samples were centrifuged at 20,000

× g for 1 min at RT. The tubes were placed in the magnetic rack and the supernatant, containing the digested proteins, was transferred to a new tube. Samples were acidified by adding formic acid to a final concentration of approximately 2% to obtain a pH < 3. Next, AttractSPE Tips RPS T1 200 µL (Affinisep) were equilibrated with 50 µL methanol centrifuged for 2 min at 1,000 × g, followed by the addition of 50 µL 0.5% acetic acid and another centrifugation. The acidified samples were loaded onto the equilibrated tips and centrifuged. Samples were washed with 30 µL and 60 µL of 0.1% formic acid and 80% acetonitrile. Samples were eluted with 65 µL of freshly prepared 5% ammonium hydroxide and 60% acetonitrile in water. Peptides were eluted by centrifugation for 3 min at 500 × g into glass vials. The elution was dried in SpeedVac set at 30°C and stored at - 20°C.

Liquid chromatography and electrospray MS

For LC-MS analysis, an UltiMate™ 3000 RSLCnano system was online coupled to an Exploris 480 mass spectrometer (both Thermo Fisher Scientific, Dreieich, Germany). The peptide mixture was washed and preconcentrated on a µPAC™ C18 trapping column (PharmaFluidics) with a flow rate of 10 µL/min and peptides were separated on a µPAC™ C18 pillar array column (50 cm bed length, PharmaFluidics) using a binary buffer system consisting of A (0.1% formic acid) and B (86% acetonitrile, 0.1% formic acid). With a flow rate of 0.5 µL/min peptides were eluted applying an isocratic gradient from 1% to 4% B in 2 min, 4% to 25% B in 24 min, 25% to 44% B in 12 min, 44% to 90% in 2 min, and 90% B for 4 min. For electrospray ionization of peptides, a Nanospray Flex ion source (Thermo Fisher Scientific) with a liquid junction PST-HV-NFU (MS Wil, The Netherlands) and a fused silica emitter (20 µm inner diameter, 360

µm outer diameter, MicroOmics Technologies LLC) with a source voltage of +1,800 V and an ion transfer tube temperature of 275°C was used. Cycles of data-independent acquisition (DIA) consisted of: one overview spectrum (RF lens of 40%, normalized AGC target of 300%, maximum injection time of 45 ms, *m/z* range of 350 to 1,400, resolution of 120,000) recorded in profile mode followed by MS2 fragment spectra (RF lens of 50%, normalized AGC target of 1000%, maximum injection time of 54 ms) generated sequentially by higher-energy collision-induced dissociation (HCD) at a normalized energy of 28% in a precursor *m/z* range from 361 to 450 in 6 windows of 14 *m/z* isolation width, in a precursor *m/z* range from 450 to 800 in 50 windows of 7 *m/z* isolation width and in a precursor *m/z* range from 800 to 1,100 in 21 windows of 14 *m/z* isolation width, overlapping by 1 *m/z* and recorded at a resolution of 30,000 in profile mode.

MS data analysis

MS raw data were converted to mzML format using the ProteoWizard software, version 3.0.21229 (Chambers *et al.* 2012). For protein and peptide identification and quantification a library free search was performed using DIA-NN version 1.8.1 (Demichev *et al.* 2020) against the organism-specific Uniprot database (release 2023_03, *Synechocystis* sp. strain PCC 6803, taxid 1148), complemented with the sequences of RNase J, 3xFLAG and GFP. Trypsin was set as protease with 2 allowed missed cleavages. Carbamidomethylation of cysteine was selected as fixed modification, N-terminal excision of methionine and oxidation of methionine were selected as variable modifications with a maximum number of 2. For precursor ion generation, peptides ranging from 7 to 35 amino acids, precursor charge from 2 to 4,

precursor *m/z* range from 361 to 1,100 and fragment ion *m/z* range from 200 to 1,200 were used. Further parameters were: match between runs, unrelated runs, search in double-pass mode, deactivated heuristic protein inference, robust LC quantification and RT-dependent cross-run normalisation. The protein group quantities output file from DIA-NN was used and all proteins with non-zero label-free quantification (LFQ) intensities in 3 out of 4 replicates in both groups were selected for further analysis. Missing values were imputed by sequential imputation using the R package impSeqRob (Verboven, Branden and Goos 2007). For differential abundance analysis, $\log_{10}$ transformed LFQ intensities were subjected to a moderated t-test using the R package limma (Ritchie *et al.* 2015) with correction of p-values for multiple testing using Benjamini and Hochberg's method.

Results

RNase J is involved in CRISPR3 crRNA maturation

We first sought to determine whether RNase J affects the maturation of CRISPR3 crRNA *in vivo*. Therefore, we cloned the *slr0551* gene encoding RNase J into the pVZ322 vector under the control of the copper-inducible *petE* promoter, P_{petE} (Zhang *et al.* 1992). We designed two different constructs: one expressing the unmodified RNase J protein, and one expressing a version with a 3×FLAG sequence fused to its C-terminal end. The constructed plasmids were conjugated into *Synechocystis* strain PCC-M (Trautmann *et al.* 2012) via tri-parental mating (Scholz *et al.* 2013). Cells were cultivated in copper-free BG11 medium and expression was induced by the addition of 2 µM Cu_2SO_4 at an OD_{750nm} of 0.8. *Synechocystis* wild type served as control. Samples were harvested over a time course of 24, 72 and 144 h post induction and

RNA was isolated for each strain. The impact of ribonuclease J overexpression on CRISPR3 crRNA maturation was analyzed through northern blot hybridization using a radioactively labeled single-stranded RNA probe spanning the CRISPR3 spacers 1 to 4. The resulting complex pattern of mature crRNAs and processing intermediates in the wild type was fully consistent with previous analyses (Scholz *et al.* 2013; Behler *et al.* 2018). The mature crRNA forms of 48 and 42 nt were among the strongest signals (**Fig. 1**). Another strong signal was obtained for the 72 nt, 144 nt and 216 nt long processing intermediates consisting of single, double and triple repeat-spacer units. Moreover, the previously reported 6 nt-periodicity (Behler *et al.* 2018) was visible in the form of the double bands for the mature crRNAs and all processing intermediates. At time point T0, prior to induction, we expected that the wild type and the two overexpression strains should show quantitatively and qualitatively similar signals. While all strains did show similar patterns, most band intensities were stronger in the strain carrying the construct for the overexpression of the untagged enzyme (*rnj* OE). Especially striking was the difference for the smaller RNA fragments, the 144 nt and shorter processing intermediates, and the mature crRNAs. This observation may be explained by the leakiness of the P_{petE} promoter. Furthermore, we noticed a slight reduction in the intensities of the signals between 100 and 250 nt in the strain encoding the tagged enzyme (*rnj-3xF* OE) (**Fig. 1**). This difference in activity between the tagged and untagged RNase J became more pronounced during the later times of the time course..

The most striking difference was seen in the disappearance of a ~70 nt band (marked by a black arrow in **Fig. 1**) in the strain overexpressing the tagged enzyme after induction. The size of the band slightly below the main signal for the single repeat-

spacer unit of 72 nt indicates that it is an crRNA maturation intermediate 2 or 3 nt shorter.

The increased signal intensities in the strain overexpressing untagged RNase J indicated that RNase J is involved in the maturation of crRNA from the subtype III-Bv CRISPR system in *Synechocystis*. Furthermore, the tagging of RNase J at its C-terminal end may have enhanced its exoribonuclease activity, explaining the overall lower crRNA signal intensities in this strain and especially the disappearance of the signal at ~70 nt at the T24, T72 and T144 time points in the strain overexpressing the tagged enzyme. Previous observations indicated an enhanced 5' exoribonuclease activity for C-terminally poly-histidine-tagged RNase J1 in *Bacillus subtilis* (Laalami and Putzer 2011), which would be consistent with the observations made here for the C-terminally tagged RNase J.

RNase J processes crRNA intermediates

We performed a primer extension to map possible processing differences between the strains overexpressing tagged and untagged RNase J. In addition, we included the *Synechocystis* δ*rnj* strain with a reduction in the number of *rnj* loci per cell (partial gene deletion) (Cavaiuolo *et al.* 2020), in which we introduced the same constructs as in the experiment in **Fig. 1**, overexpressing C-terminally tagged, or untagged RNase J. Because the partial deletion of *rnj* gene copies by insertion of a streptomycin resistance gene in the *Synechocystis* δ*rnj* strain depends on the presence of streptomycin, we used as background for all engineered strains in this experiment not the wild type, but strain WT-Spc, with a spectinomycin cassette integrated into a neutral site within the *ssl0452-slr0271* intergenic region (Cavaiuolo *et al.* 2020). A

strain carrying the empty pVZ322 vector was used as control. The cells were cultivated until reaching an OD_{750} of 0.8 and cells were collected 24 h after RNase J expression was induced. Primer extension was performed on 2 µg of total RNA using the same primer previously used to analyze the involvement of RNase E in CRISPR3 maturation (Behler *et al.* 2018). The result is shown in **Fig. 2**. The WT-Spc control strain yielded an identical pattern to previous primer extensions obtained with the *Synechocystis* wild type (Behler *et al.* 2018), indicating that the integrated resistance cassette had no effect on crRNA processing. Moreover, the two strains overexpressing RNase J or RNase J-3×FLAG showed identical patterns to the WT-Spc strain. However, two differences were apparent in the δ*rnj* strain, harboring only the empty vector. In this strain, one additional band and one band with increased intensity were observed (**Fig. 2**, arrows). While the lower band (arrow 1) was weaker, but present also in the other lanes, the upper band (arrow 2) was unique to the δ*rnj* strain (**Fig. 2**). Because in this strain the RNase J level is the lowest, this observation indicated that

a) the reduced level of RNase J in the δ*rnj* strain impacted the processing of the CRISPR3 crRNA maturation and

b) this effect was reversed when overexpressing recombinant RNase J from a plasmid.

Using the sequence ladder on the left, we identified the corresponding sequences of the observed bands. The 3’ ends of the two fragments were located close, 1 and 3 nt, to the 3’ ends of spacer 2 (S2) of the CRISPR3 array (**Fig. 2B,** arrows 1 and 2). As these two fragments accumulated in the cell, we conclude that the depletion in RNase J caused a bottleneck in the processing of the crRNA.

Previous work identified the first cleavage site of the CRISPR transcript is located at the end of the spacer, at exactly these positions, 1 to 3 nt from the first nt in the repeat

(**Fig. 2B**, arrows), leading to the 72 nt intermediate (see Fig. 3 in Scholz *et al.* (2013)). Thus, the corresponding transcript was a substrate for RNase J activity, which was limiting in this strain. As RNase J from *Synechocystis* possesses 5´ exonuclease activity (Cavaiuolo *et al.* 2020), it may then remove 2 to 4 further nucleotides from the 5´ end until reaching the stem-loop structure beginning at nt 2 of the repeat. That structure then is recognized by RNase E in a further processing step, which generates the crRNA 5´ handle (Behler *et al.* 2018).

Next, we tested the effect of RNase J on a spacer-repeat RNA substrate *in vitro*. We cloned and expressed histidine-tagged recombinant RNase J as described (Cavaiuolo *et al.* 2020). Purified RNase J was incubated with synthetic oligoribonucleotide RB24 corresponding to the CRISPR3 spacer 2-repeat sequence (substrate, 72 nt). Several weak bands were observed already in the absence of added enzyme indicating slight degradation of the substrate (background). However, a few bands clearly appeared or were increased in intensity up addition of RNase J. Especially, the more prominent signal at 35 nt (**Supplemental Fig. S1**, lane 2) is consistent with the primary cleavage at the end of the spacer as inferred from the analysis of primer extension products (**Fig. 2**), followed by exonucleolytic removal of 2 to 4 nt until reaching the stem loop located close to the 5´ end of the repeat blocking further processing, as this would yield precisely a 35 nt fragment. Thus, RNase J may have processed the synthetic RNA via its 5´ exonuclease and endonuclease activity combined.

The same experiment performed with purified RNase E provided a different cleavage pattern (**Supplemental Fig. S1**, lane 3). A prominent appearing band likely is the substrate after 13 nt were cleaved off from the 3’ end. When incubating the RNA with both ribonucleases, we obtained a cleavage pattern corresponding to the two single digestions combined (lane 4). Next, we performed analogous experiments with the 37

nt synthetic CRISPR3 repeat sequence with a single additional adenosine at the 5´ end as substrate. Incubation with RNase J or RNase E alone resulted in single additional bands with a size difference of 2 nt between the two digestions (**Supplemental Fig. S1**, lanes 6 and 7). The RNase J cleavage site thus must be close to the processing site used by RNase E to generate the 5´ handle of the CRISPR3 crRNA. The absence of a ladder-like pattern suggested that primarily the endonuclease activity of RNase J was active. Interestingly, when mixing both enzymes, we observed mainly the RNase E-related signal, i.e. the RNase J effect was almost completely suppressed (**Supplemental Fig. S1**, lane 8). This result matches the observation that *in vivo* RNase E is the dominating and rate-limiting enzyme in processing the CRISPR repeat (Behler *et al.* 2018), and accordingly, RNase J plays no significant role in cleaving the repeat.

In vivo-tagging of RNase J and characterization of proteins associating with it

We next sought to identify potential interaction partners of RNase J. Co-IP experiments were performed with *Synechocystis* strains expressing RNase J either N- or C-terminally tagged with the 3×FLAG epitope, and with GFP-expressing strains as controls (plasmids pVZ322-P_{rha}-*3×FLAG-slr0551*, pVZ322-P_{rha}-*gfp-3×FLAG*, pVZ322-P_{petE}-*slr0551-3×FLAG,* or pVZ322-P_{petE}-*gfp-3×FLAG*). The strains were cultivated in quadruplicates until an OD_{750} of approximately 9–12 was reached, and protein expression was induced for 24 h before harvesting the cells, with a final OD_{750} of approximately 25–30. Triple-FLAG tagged proteins were purified with M2 anti-FLAG magnetic beads and analyzed on by SDS-PAGE (**Supplemental Fig. S2 and S3**). Potential interaction partners were identified by mass spectrometry. In the entire

dataset, a total of 2,625 proteins was identified, corresponding to ~71.5% of the total proteome. **Supplemental Table S2** shows a detailed list of the identified proteins for each replicate.

In order to identify potential interaction partners, a $\log_2$FC threshold of +1.5 (p value ≤ 0.05) was established to select proteins which were at least 2.8-fold enriched in the RNase J overexpression strains with respect to the GFP expressing control strains. With this parameter, 27 proteins were identified for the N-terminal tagged (NTT) RNase J and 36 proteins for the C-terminal FLAG-tagged (CTT) RNase J. In both cases, RNase J, used as bait, showed the highest respective enrichment ($\log_2$FC of +10.26 and +12.13). Nine proteins were shared between the two co-IPs with the differentially tagged RNase J variants.

A gene ontology analysis was conducted to categorize the identified proteins according to their PANTHER protein class (Thomas *et al.* 2022). The most enriched proteins with the CTT RNase J were proteins in the category translation (34.30%), which represent only 3.7% of the proteins enriched in the co-IP with the NTT RNase J (**Table 1**). In the NTT RNase J, the second most prominent protein group (after unclassified) was that of metabolite interconversion enzymes. In the CTT RNase J, this category was among the smallest, comprising only 2.9%. Protein modifying enzymes constituted 14.8% of the NTT RNase J proteins, in comparison to 5.7% of the CTT RNase J proteins. Furthermore, the CTT RNase J revealed that 8.6% of the identified proteins were involved in DNA metabolism, a class of proteins that was not observed in the NTT. A significantly higher proportion of proteins (29.6%) in the NTT RNase J batch exhibited no assigned PANTHER category in comparison to the CTT RNase J batch (14.30%) (**Table 1**).

The calculated log_2FC data were plotted over the adjusted p values in the form of a volcano plot (**Fig. 3**). Among the nine proteins shared between the co-IPs with the two differentially tagged RNase J variants, PNPase stood out with log_2FC enrichment factors of +5.39 and +5.96 (**Table 2 and 3**).

PNPase is not involved in CRISPR3 crRNA maturation

PNPase was the most highly enriched ribonuclease in the RNase J co-IP (**Fig. 3A, B**). Moreover, the PNPase in *Synechocystis* forms a complex with RNase E (Zhang *et al.* 2014), therefore it was considered as another candidate for participation in the CRISPR3 crRNA maturation in *Synechocystis*. We expressed PNPase as a recombinant protein in *E. coli*, purified and tested its activity in *in vitro* cleavage assays. The samples with the successive addition of PNPase or RNase E showed the 22 and 23 nt cleavage products expected for cleavage by RNase E and remaining substrate (Behler *et al.* 2018). In all samples in which PNPase was added first, the intensity of the 36 nt substrate was lowered indicating the rapid degradation of the substrate (**Fig. 4**). Moreover, these samples showed a single nt ladder although of very low intensity, directly below the substrate. When RNase E was added first, all samples showed a stronger intensity of the 22 and the 23 nt products, likely because the entire substrate amount had been available for the cleavage by RNase E or because RNase E, when bound to the RNA, protects the substrate from the 3´exonuclease activity of PNPase. The other way around, when PNPase was added first, a part of the substrate was degraded first and only the rest of the substrate was available for the cleavage by RNase E (**Fig. 4**).

Samples incubated only with PNPase, irrespectively of incubation times and whether 1 or 3 pmol enzyme were used, showed a single nt ladder, although more substrate was degraded when more PNPase was used (**Fig. 4**, lanes to the right). We noticed that the ladder pattern was restricted to the 17 to 36 nt size range. This limitation was not an effect of the used gel conditions as the alkaline hydrolysis of the same substrate showed the ladder extending much further down. However, this result fits to the secondary structure of the CRISPR repeat used as substrate: it consists of a single stem loop from position 2 to 18, while the sequence from nt 19 to 36 is single-stranded (Behler *et al.* 2018). Hence, this result is consistent with a strong 3' exonuclease activity of the *Synechocystis* PNPase that stopped once the stem loop was reached.

Discussion

RNase J is involved in the CRISPR3 crRNA maturation

In the type III-Bv CRISPR3 system of *Synechocystis*, RNase E replaces the lacking Cas6 activity in the maturation of the pre-crRNA (Behler *et al.* 2018). Although RNase E is responsible for a major processing step, it has been suggested that additional ribonucleases are involved. While RNase E cleaves within the CRISPR3 repeat RNA, directly generating the characteristic 13 nt and 14 nt 5′ repeat handles (Behler *et al.* 2018), it does not generate the 3' ends of the mature crRNAs. Based on the analysis of mapped transcriptome reads, we previously characterized CRISPR3 crRNA maturation as a 2-step process (Scholz *et al.* 2013). This analysis revealed that the first cleavage site is located in the spacer and not in the repeat. This conclusion was supported by the observation that the 72 nt processing intermediate spans across the

493 cleavage site within the repeats and ends at the cleavage site in the spacer (Scholz *et*
494 *al.* 2013).

495 Here, we show that overexpression of RNase J correlates with an increased
496 abundance of the ~72 nt fragment, which represents a single repeat-spacer unit, of
497 other intermediates, and of the 48 nt and 42 nt mature crRNAs (**Fig. 1**). The results of
498 the primer extensions clearly identified two 5' ends that were enriched in the δ*rnj* strain
499 with decreased RNase J activity (**Fig. 2**). These results, in conjunction with the results
500 of Behler et al. (2018), suggest that RNase J mediates 5' exonucleolysis immediately
501 after the first cleavage, an endonucleolytic cleavage close to the spacer 3' ends. After
502 this, RNase E releases the mature crRNA 5' ends including the 13 or 14 nt 5′ repeat
503 handle (the 1 nt size difference in the length of the repeat handle likely results from
504 ambiguity in the substrate cleavage by RNase E itself (Behler *et al.* 2018)).

505 Looking for proteins that interact with RNase J could reveal factors that potentially
506 influence the activity or substrate recognition of RNase J, or act as an additional
507 nuclease involved in further 3' processing. Such processing is required as two mature
508 crRNA forms accumulate *in vivo*, 42 and 48 nt in length and only the latter results from
509 the combined action of RNase E and J. Therefore, we searched for proteins possibly
510 interacting with RNase J. This search identified PNPase as an enzyme strongly co-
511 enriched with RNase J (**Fig. 3**). PNPase is participating in crRNA maturation in *Listeria*
512 *monocytogenes* (Sesto *et al.* 2014) and *Bacillus subtilis* (Chou-Zheng and Hatoum-
513 Aslan 2019), which prompted us to overexpress and test PNPase from *Synechocystis*.
514 While the characterization of *Synechocystis* PNPase in an *in vitro* assay demonstrated
515 a strong 3' exonuclease activity (**Fig. 4**), we found no evidence supporting its
516 involvement in CRISPR3 maturation, at least *in vitro*. In the elution of the CTT RNase
517 J, the bifunctional nuclease domain protein Sll1142 was identified. Homologs of this

protein are conserved in cyanobacteria, and related proteins exist in many other bacteria and plants. A homolog in *Oryza minuta* was reported to possess bifunctional RNase and DNase activities *in vitro* (You *et al.* 2010). However, whether Sll1142 has any CRISPR-related function remains to be elucidated.

The here described involvement of RNase J in the maturation of CRISPR3 crRNAs adds further evidence on the connection between degradosome components and the type III CRISPR-Cas machinery (Behler *et al.* 2018; Chou-Zheng and Hatoum-Aslan 2019; Bilger *et al.* 2024). Our current model for CRISPR3 crRNA maturation is shown in **Fig. 5**.

Co-IP analysis indicates the existence of a degradosome in *Synechocystis* involving RNase J

We identified several potential interaction partners for the bifunctional endo- and exoribonuclease RNase J in *Synechocystis*. We conducted a co-IP experiment with N- or C-terminal 3×FLAG-tagged RNase J. The results revealed a significant difference between the two pull-downs. In addition to RNase J, 35 enriched proteins were identified for the CTT RNase J and 26 proteins for the NTT RNase J. Notably, only nine proteins were enriched in both co-IPs. This discrepancy suggests that the presence and position of the 3×FLAG tag on RNase J was a relevant factor.

The composition of RNA degradosomes varies considerably between different species (Tejada-Arranz, Crécy-Lagard and Reuse 2020; Zhang, Hess and Zhang 2022). The majority of degradosomes contain at least one major RNase (either RNase E, J or Y) and an RNA helicase (Tejada-Arranz, Crécy-Lagard and Reuse 2020). In the

cyanobacteria *Nostoc* (*Anabaena*) sp. PCC 7120 and *Synechocystis*, RNase E forms a complex with PNPase, wherein the latter recognizes a conserved nonapeptide RRRRRRSSA at the end of RNase E (RRRRRSSA in *Synechocystis*) (Zhang *et al.* 2014). In our study, RNase E was not enriched in comparison to the GFP control. However, PNPase was one of the most enriched proteins in both, CTT and NTT RNase J co-IPs. These data suggest that PNPase may form degradosomes with either RNase E or RNase J. It is noteworthy that RNase J carries a conserved arginine-rich motif close to its C terminus (RRSRKRS in *Synechocystis*), as is found in RNase E. This led us perform structure prediction of RNase J with PNPase using Alphafold 3 (Abramson *et al.* 2024). Alphafold 3 rendered five structures, four of which showed a potential interaction between the arginine-rich motif of RNase J and PNPase (**Fig. 6**). The residues that are likely to bind PNPase to the C-terminal domain (CTD) of RNase J were compared with previously identified interaction sites of PNPase and RNase E in *E. coli* (Durán-Figueroa *et al.* 2006). The residues from our prediction were all located within the interaction domain of PNPase, indicating that the same region is responsible for the interaction, though *E. coli* RNase E does not possess the arginine-rich motif from *Synechocystis* RNase E or RNase J (**Supplemental Fig. S4**). In *Synechocystis,* PNPase may form a complex with either RNase E or RNase J, but it is not possible to conclude which interaction is favored under standard growth conditions, as the overexpression of RNase J in the cell may have favored the binding of PNPase to ribonuclease J. In *M. tuberculosis*, putative core RNA degradosome elements were predicted to be PNPase, RNase E, RNase J, and RNA helicase RhlE (Płociński *et al.* 2019). Similarly, the *Bacillus subtilis* degradosome is built around RNase Y, interacting with PNPase, the helicase CshA and the glycolytic enzymes enolase and PfkA (Lehnik-Habrink *et al.* 2010). These studies have shown that the

composition of the RNA degradosome is complex and that the interactions of the enzymes involved in RNA degradation in *B. subtilis* are also rapidly changing (Cascante-Estepa, Gunka and Stülke 2016). Therefore, it cannot be excluded that *Synechocystis* RNase E and RNase J may both together, or alternatively, be part of the complex, via PNPase, or other factors.

While we identified RNase J as part of the machinery enabling the maturation of CRISPR3 crRNA in the absence of Cas6 enzymes, we were unable to identify enriched Cas proteins from the CRISPR3 effector complex. This indicates that RNase J does not perform an interaction with the effector complex, or that the crRNA is loaded into the Cmr effector complex at a later stage.

The diversity of protein types identified in our data suggests the involvement of RNase J in a multitude of pathways. Three proteins, namely DNA topoisomerase 1, RecA and single-stranded DNA binding protein (ssb) point towards a potential role in DNA repair and replication. Moreover, we identified several transcription factors, such as the RuBisCO transcriptional regulator (Bolay *et al.* 2022), the response regulator Rre1, the major nitrogen-related regulator NtcA, and the AbrB-like transcription regulator Sll0822, also involved in nitrogen-related regulation (Ishii and Hihara 2008), .

In *E. coli* and many other bacteria, enolase, a glycolytic enzyme, is a component of the degradosome complex (Vanzo *et al.* 1998; Domínguez-Malfavón *et al.* 2013) establishing a connection between RNA degradation and glycolysis. In *B. subtilis*, RNase J1 interacts with enolase and phosphofructokinase (Commichau *et al.* 2009). In our co-IP experiment, we identified pyruvate kinase (**Table 2**), which catalyzes the final reaction in glycolysis by converting phosphoenolpyruvate into pyruvate. It would be worth investigating why in three different degradosome systems, different glycolytic

enzymes were found. In *E. coli,* the degradosome associated enolase plays a role in the regulation of the stability of the *ptsG* mRNA, encoding the major glucose transporter, during metabolic stress (Morita *et al.* 2004).

The Slr1102 protein was with a $\log_2$FC of +5.39 one of the most highly enriched proteins in the NTT RNase J co-IP (**Table 2**). Slr1102 possesses a multiple domain structure including a FHA, two PAS, an EAL, and a partially degenerate GGDEF domain (Enomoto, Wallner and Wilde 2023), suggesting involvement in light-dependent cyclic di-GMP-mediated signaling processes. Cyclic di-GMP is also involved in bacterial stress responses (Wang *et al.* 2023), which concurs with the identification of Slr0244 (containing a universal stress protein, UspA domain) and the response regulator Rre1, which is expressed in response to heat stress (Kobayashi *et al.* 2017). Furthermore, Rre1 is regulated by TrxA (Ibrahim *et al.* 2022), which was found to be enriched in the CTT RNase J co-IP. Taken together, this draws a picture that RNase J might be involved in stress responses that require ribonucleases to degrade transcripts that are no longer needed.

One uncharacterized protein that was enriched in both RNase J co-IPs was Slr0552. This is of interest because RNase J (Slr0551) and Slr0552 are encoded by two genes in the same operon. A BlastP search and structural analysis by Foldseek revealed that homologs exist in cyanobacteria and other organisms**.** The genomic neighborhood of *slr0552* and *slr0551* suggests that both proteins may interact with each other. Moreover, synteny analysis of the genomic organization of *rnj* and *slr0552* homologs show a conserved synteny in the *Synechocystis* genus and also in more distantly related cyanobacteria like *Gloeothece* and *Crocosphaera* (**Supplementary Fig. S5)**. The function of Slr0552 and its relationship to RNase J remains a subject for future investigation.

Data availability

MS proteomics data have been deposited to the ProteomeXchange Consortium via the PRIDE partner repository (Perez-Riverol *et al.* 2025) and are available through the identifier PXD060866.

Funding

This work was supported by the German Research Foundation priority program SPP2141 (grant HE 2544/14-2 to WRH).

Acknowledgments

We thank Viktoria Reimann, Freiburg, for the 5S rRNA hybridization in **Fig. 1** and Juliane Behler, Freiburg, for helpful comments in an early phase of the project.

Author contributions

WRH designed the project and secured funding. FD, BK and PH carried out MS-based proteomic analyses. TB carried out all PNPase-related experiments, HL contributed to the co-IP analyses, all other experiments were performed by RB. Data were analyzed by RB, FD, HP and WRH; RB and WRH wrote the manuscript with input from all authors.

References

Abramson J, Adler J, Dunger J *et al.* Accurate structure prediction of biomolecular interactions with AlphaFold 3. *Nature* 2024;**630**:493–500.

Aït-Bara S, Carpousis AJ. RNA degradosomes in bacteria and chloroplasts: classification, distribution and evolution of RNase E homologs. *Molecular Microbiology* 2015;**97**:1021–135.

Alifano P, Bruni CB, Carlomagno MS. Control of mRNA processing and decay in prokaryotes. *Genetica* 1994;**94**:157–72.

Behler J, Sharma K, Reimann V *et al.* The host-encoded RNase E endonuclease as the crRNA maturation enzyme in a CRISPR–Cas subtype III-Bv system. *Nat Microbiol* 2018;**3**:367–77.

Beyer HM, Gonschorek P, Samodelov SL *et al.* AQUA cloning: a versatile and simple enzyme-free cloning approach. *PLOS ONE* 2015;**10**:e0137652.

Bilger R, Migur A, Wulf A *et al.* A type III-Dv CRISPR-Cas system is controlled by the transcription factor RpaB and interacts with the DEAD-box RNA helicase CrhR. *Cell Reports* 2024;**43**, DOI: 10.1016/j.celrep.2024.114485.

Bolay P, Schlüter S, Grimm S *et al.* The transcriptional regulator RbcR controls ribulose-1,5-bisphosphate carboxylase/oxygenase (RuBisCO) genes in the cyanobacterium *Synechocystis* sp. PCC 6803. *New Phytol* 2022;**235**:432–45.

Callebaut I, Moshous D, Mornon J *et al.* Metallo-β-lactamase fold within nucleic acids processing enzymes: the β-CASP family. *Nucleic Acids Research* 2002;**30**:3592–601.

Cascante-Estepa N, Gunka K, Stülke J. Localization of components of the RNA-degrading machine in *Bacillus subtilis*. *Front Microbiol* 2016;**7**, DOI: 10.3389/fmicb.2016.01492.

Cavaiuolo M, Chagneau C, Laalami S *et al.* Impact of RNase E and RNase J on global mRNA metabolism in the cyanobacterium *Synechocystis* PCC6803. *Front Microbiol* 2020;**11**:1055.

Chambers MC, Maclean B, Burke R *et al.* A cross-platform toolkit for mass spectrometry and proteomics. *Nat Biotechnol* 2012;**30**:918–20.

Chao Y, Li L, Girodat D *et al. In Vivo* cleavage map illuminates the central role of RNase E in coding and non-coding RNA pathways. *Mol Cell* 2017;**65**:39–51.

Chen H, Zou W, Zhao J. Ribonuclease J is required for chloroplast and embryo development in Arabidopsis. *Journal of Experimental Botany* 2015;**66**:2079–91.

Chou-Zheng L, Hatoum-Aslan A. A type III-A CRISPR-Cas system employs degradosome nucleases to ensure robust immunity. *eLife* 2019;**8**, DOI: 10.7554/eLife.45393.

Commichau FM, Rothe FM, Herzberg C *et al.* Novel activities of glycolytic enzymes in Bacillus subtilis: interactions with essential proteins involved in mRNA processing. *Mol Cell Proteomics* 2009;**8**:1350–60.

Condon C, Gilet L. The metallo-β-lactamase family of ribonucleases. In: Nicholson AW (ed.), *Ribonucleases*. Berlin, Heidelberg: Springer, 2011, 245–67.

Deana A, Belasco JG. Lost in translation: the influence of ribosomes on bacterial mRNA decay. *Genes Dev* 2005;**19**:2526–33.

Demichev V, Messner CB, Vernardis SI *et al.* DIA-NN: neural networks and interference correction enable deep proteome coverage in high throughput. *Nat Methods* 2020;**17**:41–4.

Domínguez-Malfavón L, Islas LD, Luisi BF *et al.* The assembly and distribution *in vivo* of the *Escherichia coli* RNA degradosome. *Biochimie* 2013;**95**:2034–41.

Durán-Figueroa NV, Piña-Escobedo A, Schroeder I *et al.* Polynucleotide phosphorylase interacts with ribonuclease E through a ββαββα domain. *Biochimie* 2006;**88**:725–35.

Ehretsmann CP, Carpousis AJ, Krisch HM. Specificity of *Escherichia coli* endoribonuclease RNase E: *in vivo* and *in vitro* analysis of mutants in a bacteriophage T4 mRNA processing site. *Genes Dev* 1992;**6**:149–59.

Enomoto G, Wallner T, Wilde A. Control of light-dependent behaviour in cyanobacteria by the second messenger cyclic di-GMP. *Microlife* 2023;**4**:uqad019.

Even S, Pellegrini O, Zig L *et al.* Ribonucleases J1 and J2: two novel endoribonucleases in *B. subtilis* with functional homology to *E. coli* RNase E. *Nucleic Acids Res* 2005;**33**:2141–52.

Hasenöhrl D, Konrat R, Bläsi U. Identification of an RNase J ortholog in *Sulfolobus solfataricus*: Implications for 5′-to-3′ directional decay and 5′-end protection of mRNA in Crenarchaeota. *RNA* 2011;**17**:99–107.

Hemm L, Miucci A, Kraus A *et al.* Interactors and effects of overexpressing YlxR/RnpM, a conserved RNA binding protein in cyanobacteria. *RNA Biol* 2024;**21**:1–19.

Hoffmann UA, Heyl F, Rogh SN *et al.* Transcriptome-wide *in vivo* mapping of cleavage sites for the compact cyanobacterial ribonuclease E reveals insights into its function and substrate recognition. *Nucleic Acids Res* 2021;**49**:13075–91.

Hoffmann UA, Lichtenberg E, Rogh SN *et al.* The role of the 5’ sensing function of ribonuclease E in cyanobacteria. *RNA Biol* 2024;**21**:1–18.

Hotto AM, Stern DB, Schuster G. Plant Ribonuclease J: An essential player in maintaining chloroplast RNA quality control for gene expression. *Plants* 2020;**9**:334.

Hughes CS, Moggridge S, Müller T *et al.* Single-pot, solid-phase-enhanced sample preparation for proteomics experiments. *Nat Protoc* 2019;**14**:68–85.

Ibrahim IM, Rowden SJL, Cramer WA *et al.* Thiol redox switches regulate the oligomeric state of cyanobacterial Rre1, RpaA and RpaB response regulators. *FEBS Lett* 2022;**596**:1533–43.

Ishii A, Hihara Y. An AbrB-like transcriptional regulator, Sll0822, is essential for the activation of nitrogen-regulated genes in *Synechocystis* sp. PCC 6803. *Plant Physiology* 2008;**148**:660–70.

Kaltenbrunner A, Reimann V, Hoffmann UA *et al.* Regulation of pSYSA defense plasmid copy number in *Synechocystis* through RNase E and a highly transcribed asRNA. *Frontiers in Microbiology* 2023;**14**:1112307.

Kelly CL, Taylor GM, Hitchcock A *et al.* A rhamnose-inducible system for precise and temporal control of gene expression in cyanobacteria. *ACS Synth Biol* 2018;**7**:1056–66.

Kelly CL, Taylor GM, Šatkutė A *et al.* Transcriptional terminators allow leak-free chromosomal integration of genetic constructs in cyanobacteria. *Microorganisms* 2019;**7**:263.

Kieper SN, Almendros C, Behler J *et al.* Cas4 facilitates PAM-compatible spacer selection during CRISPR adaptation. *Cell Reports* 2018;**22**:3377–338.

Kobayashi I, Watanabe S, Kanesaki Y *et al.* Conserved two-component Hik34-Rre1 module directly activates heat-stress inducible transcription of major chaperone and other genes in *Synechococcus elongatus* PCC 7942. *Mol Microbiol* 2017;**104**:260–77.

Laalami S, Putzer H. mRNA degradation and maturation in prokaryotes: the global players. 2011;**2**:491–506.

Laalami S, Zig L, Putzer H. Initiation of mRNA decay in bacteria. *Cell Mol Life Sci* 2014;**71**:1799–828.

Lehnik-Habrink M, Newman J, Rothe FM *et al.* RNase Y in *Bacillus subtilis*: a natively dsordered protein that is the functional equivalent of RNase E from *Escherichia coli*. *J Bacteriol* 2011;**193**:5431–41.

Lehnik-Habrink M, Pförtner H, Rempeters L *et al.* The RNA degradosome in *Bacillus subtilis*: identification of CshA as the major RNA helicase in the multiprotein complex. *Molecular Microbiology* 2010;**77**:958–71.

Levy S, Portnoy V, Admon J *et al.* Distinct activities of several RNase J proteins in methanogenic archaea. *RNA Biology* 2011;**8**:1073–83.

Liponska A, Jamalli A, Kuras R *et al.* Tracking the elusive 5’ exonuclease activity of *Chlamydomonas reinhardtii* RNase J. *Plant Mol Biol* 2018;**96**:641–53.

Liu S-J, Lin G-M, Yuan Y-Q *et al.* A conserved protein inhibitor brings under check the activity of RNase E in cyanobacteria. *Nucleic Acids Res* 2024;**52**:404–19.

Mackie GA. RNase E: at the interface of bacterial RNA processing and decay. *Nat Rev Microbiol* 2013;**11**:45–57.

Marincola G, Schäfer T, Behler J *et al.* RNase Y of *Staphylococcus aureus* and its role in the activation of virulence genes. *Molecular Microbiology* 2012;**85**:817–32.

Mathy N, Bénard L, Pellegrini O *et al.* 5′-to-3′ exoribonuclease activity in bacteria: role of RNase J1 in rRNA maturation and 5′ stability of mRNA. *Cell* 2007;**129**:681–92.

McBride TM, Schwartz EA, Kumar A *et al.* Diverse CRISPR-Cas complexes require independent translation of small and large subunits from a single gene. *Molecular Cell* 2020;**80**:971–9.

Migur A, Heyl F, Fuss J *et al.* The temperature-regulated DEAD-box RNA helicase CrhR interactome: autoregulation and photosynthesis-related transcripts. 2021:16.

Morita T, Kawamoto H, Mizota T *et al.* Enolase in the RNA degradosome plays a crucial role in the rapid decay of glucose transporter mRNA in the response to phosphosugar stress in *Escherichia coli*. *Mol Microbiol* 2004;**54**:1063–75.

Newman JA, Hewitt L, Rodrigues C *et al.* Dissection of the network of interactions that links RNA processing with glycolysis in the *Bacillus subtilis* degradosome. *J Mol Biol* 2012;**416**:121–36.

Perez-Riverol Y, Bandla C, Kundu DJ *et al.* The PRIDE database at 20 years: 2025 update. *Nucleic Acids Res* 2025;**53**:D543–53.

Pinto FL, Thapper A, Sontheim W *et al.* Analysis of current and alternative phenol based RNA extraction methodologies for cyanobacteria. *BMC Mol Biol* 2009;**10**:79.

Płociński P, Macios M, Houghton J *et al.* Proteomic and transcriptomic experiments reveal an essential role of RNA degradosome complexes in shaping the transcriptome of *Mycobacterium tuberculosis*. *Nucleic Acids Res* 2019;**47**:5892–905.

Redko Y, Aubert S, Stachowicz A *et al.* A minimal bacterial RNase J-based degradosome is associated with translating ribosomes. *Nucleic Acids Research* 2013;**41**:288–301.

Reimann V, Alkhnbashi OS, Saunders SJ *et al.* Structural constraints and enzymatic promiscuity in the Cas6-dependent generation of crRNAs. *Nucleic Acids Research* 2017;**45**:915–25.

Rippka R, Deruelles J, Waterbury JB *et al.* Generic assignments, strain histories and properties of pure cultures of cyanobacteria. *Microbiology* 1979;**111**:1–61.

Ritchie ME, Phipson B, Wu D *et al.* limma powers differential expression analyses for RNA-sequencing and microarray studies. *Nucleic Acids Res* 2015;**43**:e47.

Scholz I, Lange SJ, Hein S *et al.* CRISPR-Cas systems in the cyanobacterium *Synechocystis* sp. PCC6803 exhibit distinct processing pathways involving at least two Cas6 and a Cmr2 protein. *PLoS ONE* 2013;**8**:e56470.

Scholz I, Lott SC, Behler J *et al.* Divergent methylation of CRISPR repeats and cas genes in a subtype I-D CRISPR-Cas-system. *BMC Microbiology* 2019;**19**:147.1-147.11.

Schwartz EA, Bravo JPK, Ahsan M *et al.* RNA targeting and cleavage by the type III-Dv CRISPR effector complex. *Nat Commun* 2024;**15**:3324.

Scornet AL, Jousselin A, Baumas K *et al.* Critical factors for precise and efficient RNA cleavage by RNase Y in *Staphylococcus aureus*. *PLOS Genetics* 2024;**20**:e1011349.

Sesto N, Touchon M, Andrade JM *et al.* A PNPase dependent CRISPR System in *Listeria*. *PLoS Genet* 2014;**10**:e1004065.

Shahbabian K, Jamalli A, Zig L *et al.* RNase Y, a novel endoribonuclease, initiates riboswitch turnover in *Bacillus subtilis*. *The EMBO Journal* 2009;**28**:3523–33.

Tejada-Arranz A, Crécy-Lagard V de, Reuse H de. Bacterial RNA degradosomes: molecular machines under tight control. *Trends in Biochemical Sciences* 2020;**45**:42–57.

Thomas PD, Ebert D, Muruganujan A *et al.* PANTHER: Making genome-scale phylogenetics accessible to all. *Protein Science* 2022;**31**:8–22.

Trautmann D, Voß B, Wilde A *et al.* Microevolution in cyanobacteria: re-sequencing a motile substrain of *Synechocystis* sp. PCC 6803. *DNA Res* 2012;**19**:435–48.

Vanzo NF, Li YS, Py B *et al.* Ribonuclease E organizes the protein interactions in the *Escherichia coli* RNA degradosome. *Genes Dev* 1998;**12**:2770–81.

Verboven S, Branden KV, Goos P. Sequential imputation for missing values. *Comput Biol Chem* 2007;**31**:320–7.

Wang Z, Song L, Liu X *et al.* Bacterial second messenger c-di-GMP: Emerging functions in stress resistance. *Microbiological Research* 2023;**268**:127302.

Yan H, Qin X, Wang L *et al.* Both enolase and the DEAD-Box RNA helicase CrhB can form complexes with RNase E in *Anabaena* sp. strain PCC 7120. *Appl Environ Microbiol* 2020;**86**:e00425-20.

Yegorov Y, Sendersky E, Zilberman S *et al.* A cyanobacterial component required for pilus biogenesis affects the exoproteome. *mBio* 2021;**12**:10.1128/mbio.03674-20.

Yoshihara S, Suzuki F, Fujita H *et al.* Novel putative photoreceptor and regulatory genes required for the positive phototactic movement of the unicellular motile cyanobacterium *Synechocystis* sp. PCC 6803. *Plant and Cell Physiology* 2000;**41**:1299–304.

You MK, Shin HY, Kim YJ *et al.* Novel bifunctional nucleases, OmBBD and AtBBD1, are involved in abscisic acid-mediated callose deposition in *Arabidopsis*. *Plant Physiol* 2010;**152**:1015–29.

Zerulla K, Ludt K, Soppa J. The ploidy level of *Synechocystis* sp. PCC 6803 is highly variable and is influenced by growth phase and by chemical and physical external parameters. *Microbiology (Reading, Engl)* 2016;**162**:730–9.

Zhang J, Hess WR, Zhang C. “Life is short, and art is long”: RNA degradation in cyanobacteria and model bacteria. *mLife* 2022;**1**:21–39.

Zhang J-Y, Deng X-M, Li F-P *et al.* RNase E forms a complex with polynucleotide phosphorylase in cyanobacteria via a cyanobacterial-specific nonapeptide in the noncatalytic region. *RNA* 2014;**20**:568–79.

Zhang L, McSpadden B, Pakrasi HB *et al.* Copper-mediated regulation of cytochrome c553 and plastocyanin in the cyanobacterium *Synechocystis* 6803. *J Biol Chem* 1992;**267**:19054–9.

Zheng X, Feng N, Li D *et al.* New molecular insights into an archaeal RNase J reveal a conserved processive exoribonucleolysis mechanism of the RNase J family. *Molecular Microbiology* 2017;**106**:351–66.

Zhou C, Zhang J, Hu X *et al.* RNase II binds to RNase E and modulates its endoribonucleolytic activity in the cyanobacterium *Anabaena* PCC 7120. *Nucleic Acids Research* 2020;**48**:3922–34.

Zinchenko VV, Piven IV, Melnik VA *et al.* Vectors for the complementation analysis of cyanobacterial mutants. *Russian Journal of Genetics* 1999;**35**:228–32.

Figures

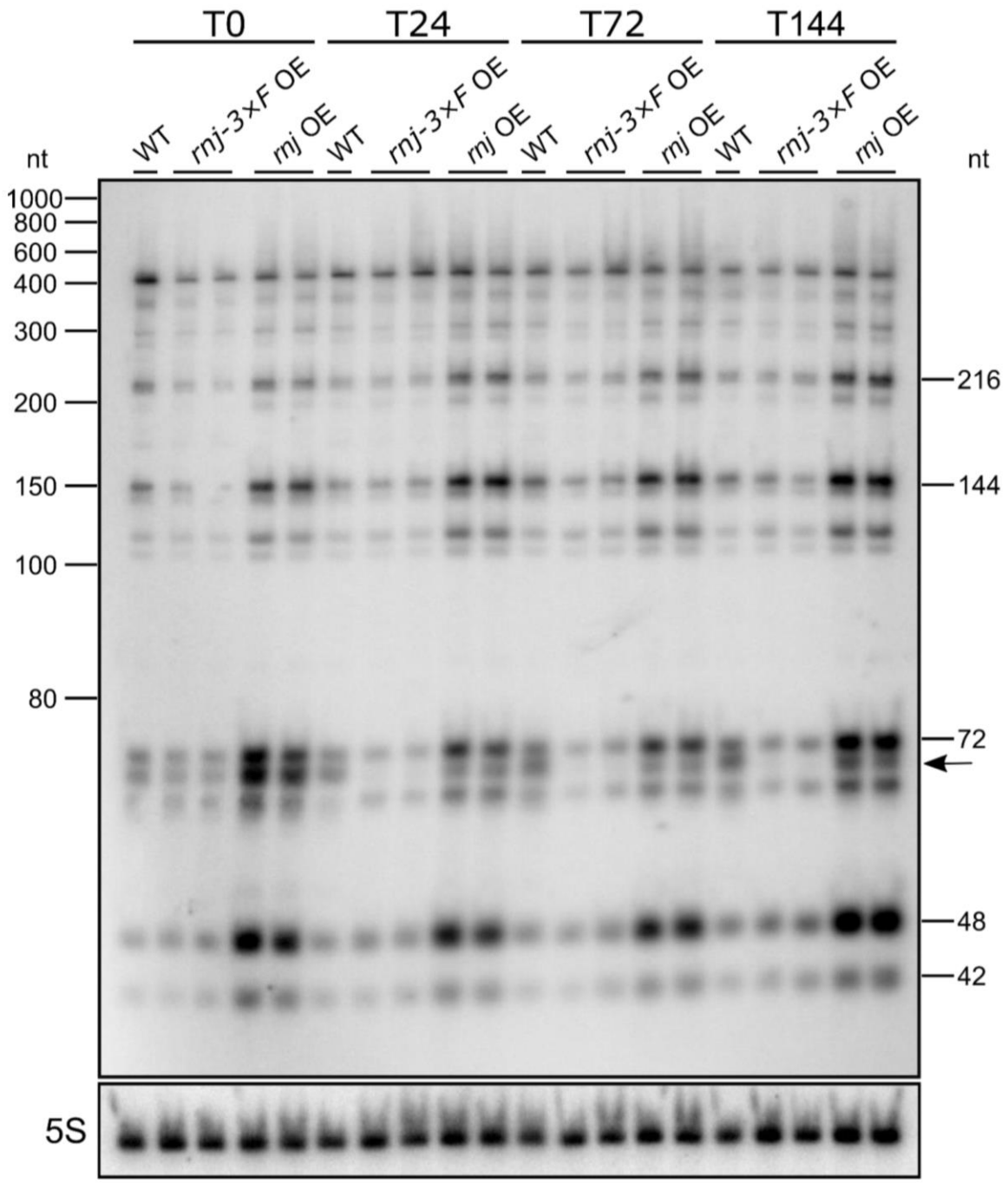

Figure 1. CRISPR 3 crRNA accumulation in *Synechocystis* wild type and RNase J overexpression strains. The strains carrying pVZ322-P_{petE} constructs for the expression of RNase J (*rnj* OE) or RNase J-3×FLAG (*rnj* x3F OE) and the wild type strain (WT) were cultivated in copper-free BG11 medium until reaching an OD_{750} of

0.8. Expression of RNase J was induced with 2 µM $CuSO_4$. Samples of the cultures were collected before induction (T0), and 24 h, 72 h and 144 h after induction. Ten µg of total RNA isolated from each culture was separated on an 8.3M urea - 10% PAA gel. For Northern hybridization, a ^{32}P-labelled transcript probe was used spanning CRISPR 3 spacers 1 - 4. Hybridization of 5S rRNA is shown as the control for equal loading. The black arrow marks the band at approximately 70 nt that is referred to in the text.

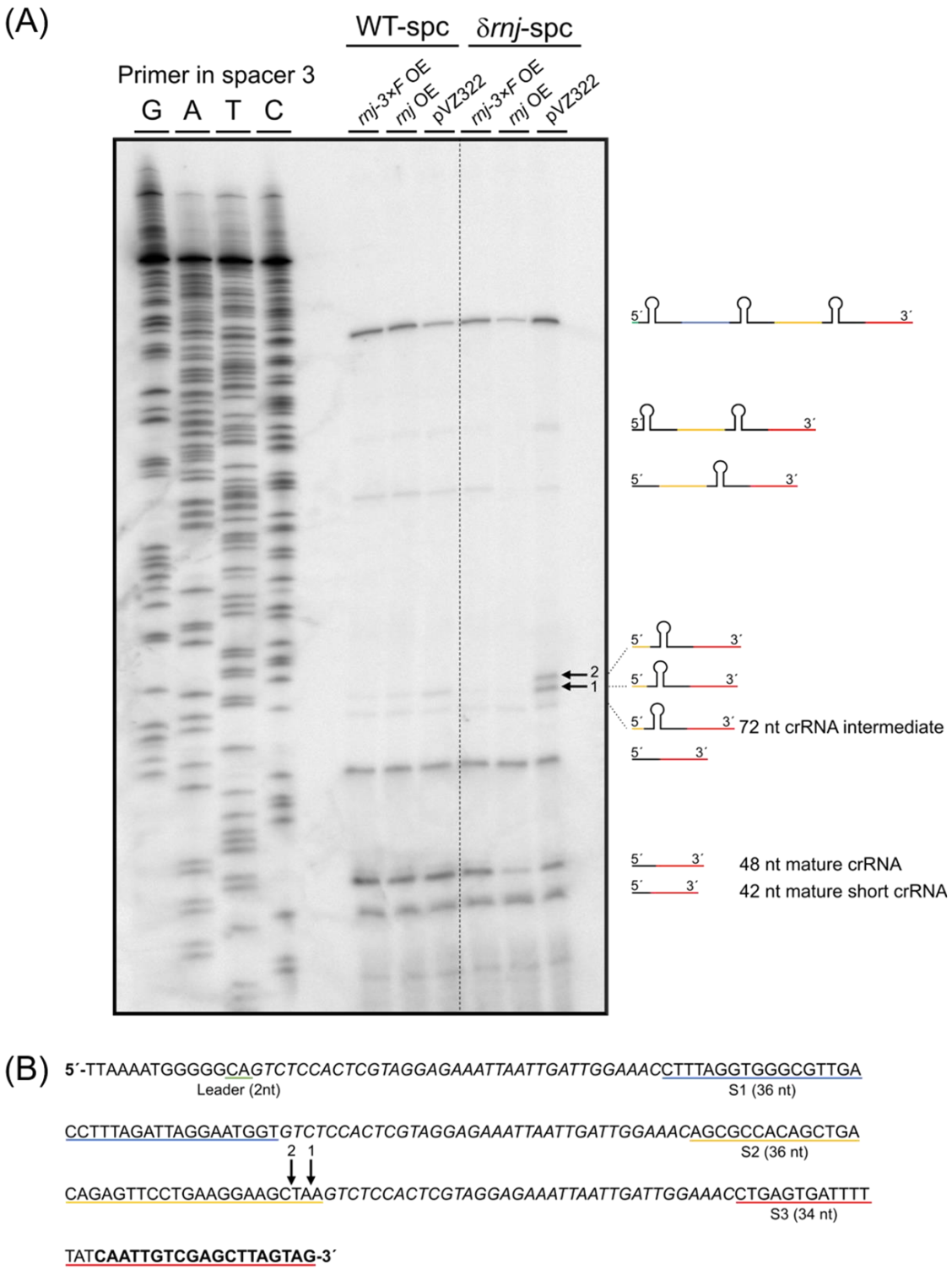

Figure 2. Mapping of RNase J in vivo processing sites within CRISPR3 pre-crRNA by primer extension. Total RNA was isolated from the *Synechocystis rnj* (*slr0551*) knock-down strain δ*rnj* carrying the empty vector pVZ322 as control, pVZ322-P*petE-slr0551*, or pVZ322-P*petE-slr0551-3×flag*, as well as the

Synechocystis wild type with integrated spectinomycin cassette (WT-Spc) and carrying the same set of plasmid constructs as δ*rnj*. The RNA was subjected to primer extension analysis using the 5´-end-labelled oligonucleotide primer Ext_S3_rev (**Table S1**) and 2 µg of total RNA per reaction. Primer extension products were separated on 8.3 M urea-15% PAA gels cast in a sequencing gel device. **(A)** Mapping of *in vivo* cleavage within CRISPR3 revealed the stronger accumulation of two fragments in the δ*rnj* strain with decreased RNase J expression (pVZ322), labeled by arrows 1 and 2. **(B)** Section of the CRISPR3 repeat-spacer array nucleotide sequence, corresponding to the mapped region. The binding site of the labeled primer in spacer 3 necessary for reverse transcription is shown in bold. The sequence of the CRISPR3 repeats are in italics. The sequences of the spacers are underlined in blue for spacer 1 (S1), in yellow for spacer 2 (S2) and in red for spacer 3 (S3), with the length of the corresponding spacer in parentheses. The sequence of the 2 nt long leader is underlined in green. The cleavage sites attributed to RNase J are marked by black arrows labelled 1 for the +1 and 2 for the + 3 cleavage sites close to the end of spacer 2.

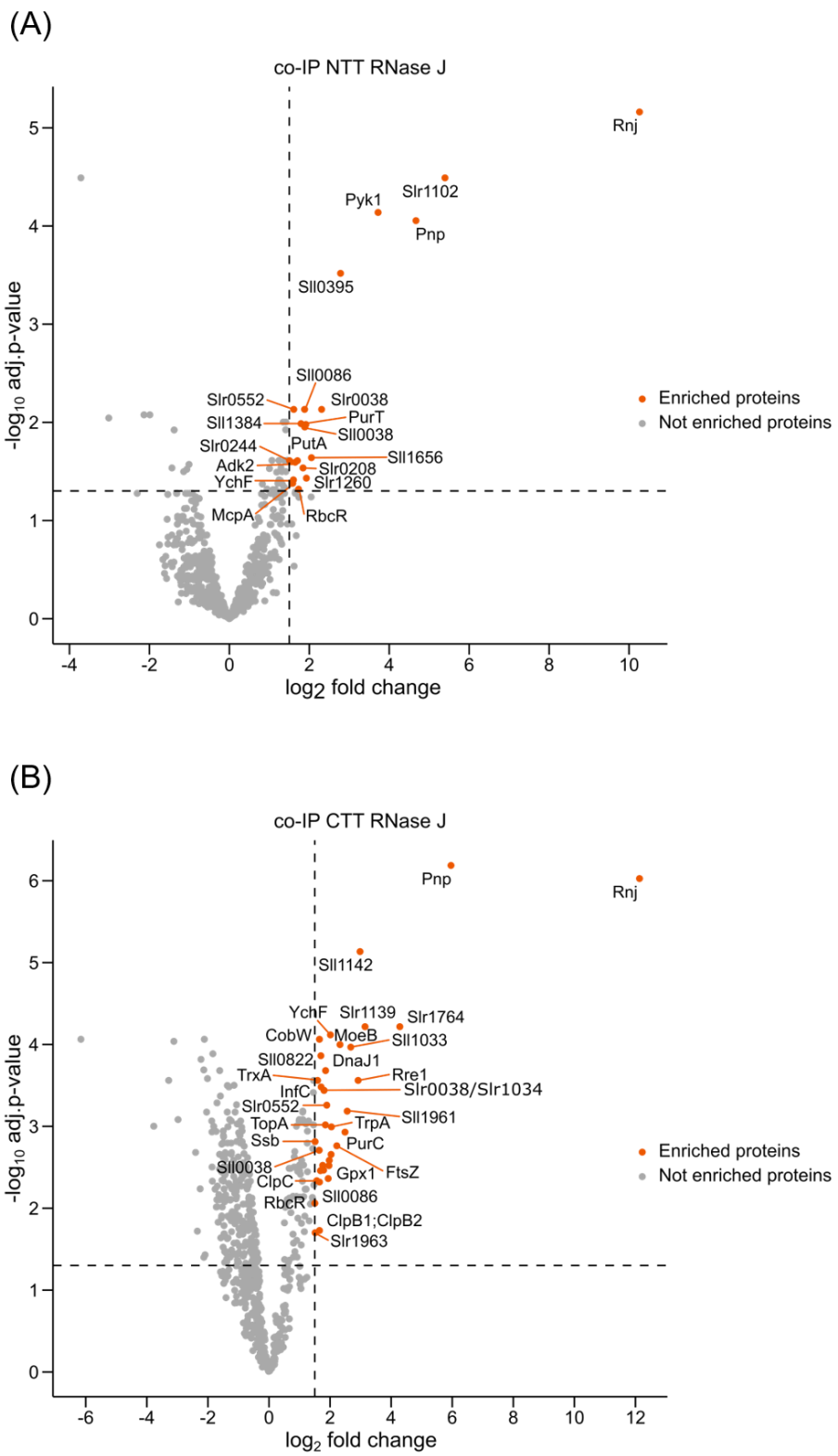

Figure 3. Co-IP experiment for the identification of interaction partners of RNase J. *Synechocystis* strains carrying pVZ322 constructs for the expression of RNase J with N- or C-terminal 3×FLAG tag, under the control of rhamnose or *petE* promoter,

respectively, were cultivated in the CellDEG high density system. *Synechocystis* strains overexpressing GFP-3×FLAG under the control of the same promoters were used as control. Protein expression was induced after 48 h of cultivation with 6 mg/ml L-rhamnose or 2 µM $CuSO_4$. The equivalent of 1000 OD cells was harvested. FLAG-tagged proteins were purified with M2 anti-FLAG magnetic beads and co-enriched proteins were analyzed by mass spectrometry. Proteins detected in the RNase J elution fraction were compared with the corresponding GFP control and visualized as volcano plots based on a Limma moderated t-test with adjustment for multiple testing correction. The thresholds for p value and $\log_2$ fold change ($\log_2$FC) were set to 0.05 and 1.5, respectively. Proteins with significant enrichment are indicated by orange dots (enriched), while proteins which did not match the selection criteria are shown in light grey (not enriched). **(A)** Co-IP with NTT RNase J. **(B)** Co-IP with CTT RNase J. The annotations and additional details of the enriched proteins are provided in **Table 2** and **Table 3**.

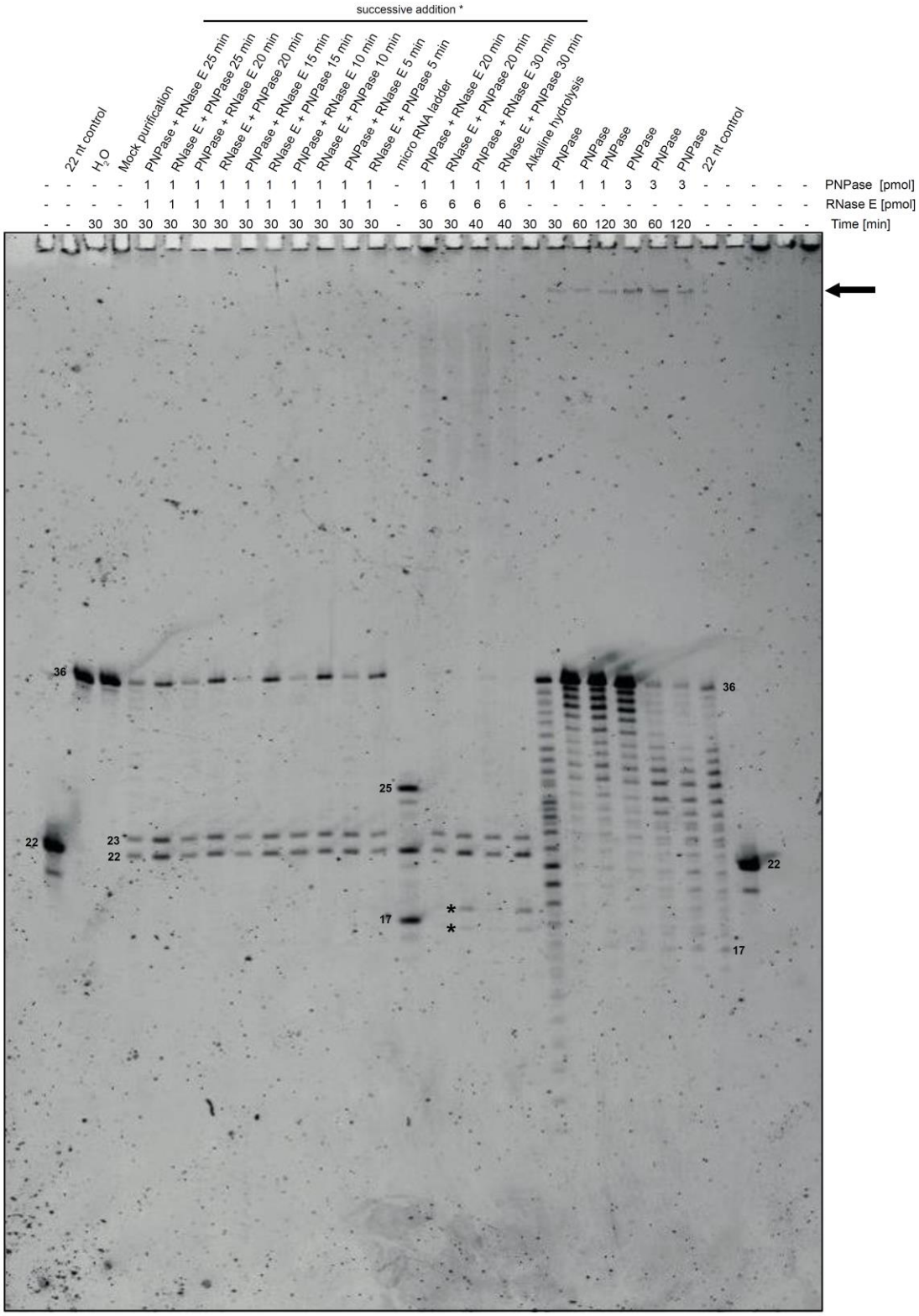

904

905 **Figure 4. *In vitro* cleavage assays with PNPase and RNase E.** Different
906 concentrations of each enzyme were used. The 5'-P CRISPR3 repeat RNA
907 oligonucleotide was used as substrate (100 ng per reaction) at 30°C with the indicated

enzyme amounts and incubation times. The first enzyme was added directly at the beginning and the second enzyme was added after the time indicated behind. 8 M urea - 15% PAA gels were used and stained with SYBR Gold. The Micro RNA ladder (NEB) served as size marker. All sizes given in nt. Nuclease-free water and the mock purification served as negative controls. A black arrow refers to unusual high molecular products. Asterisks label unspecific products resulting from high RNase E concentrations if this enzyme was added first.

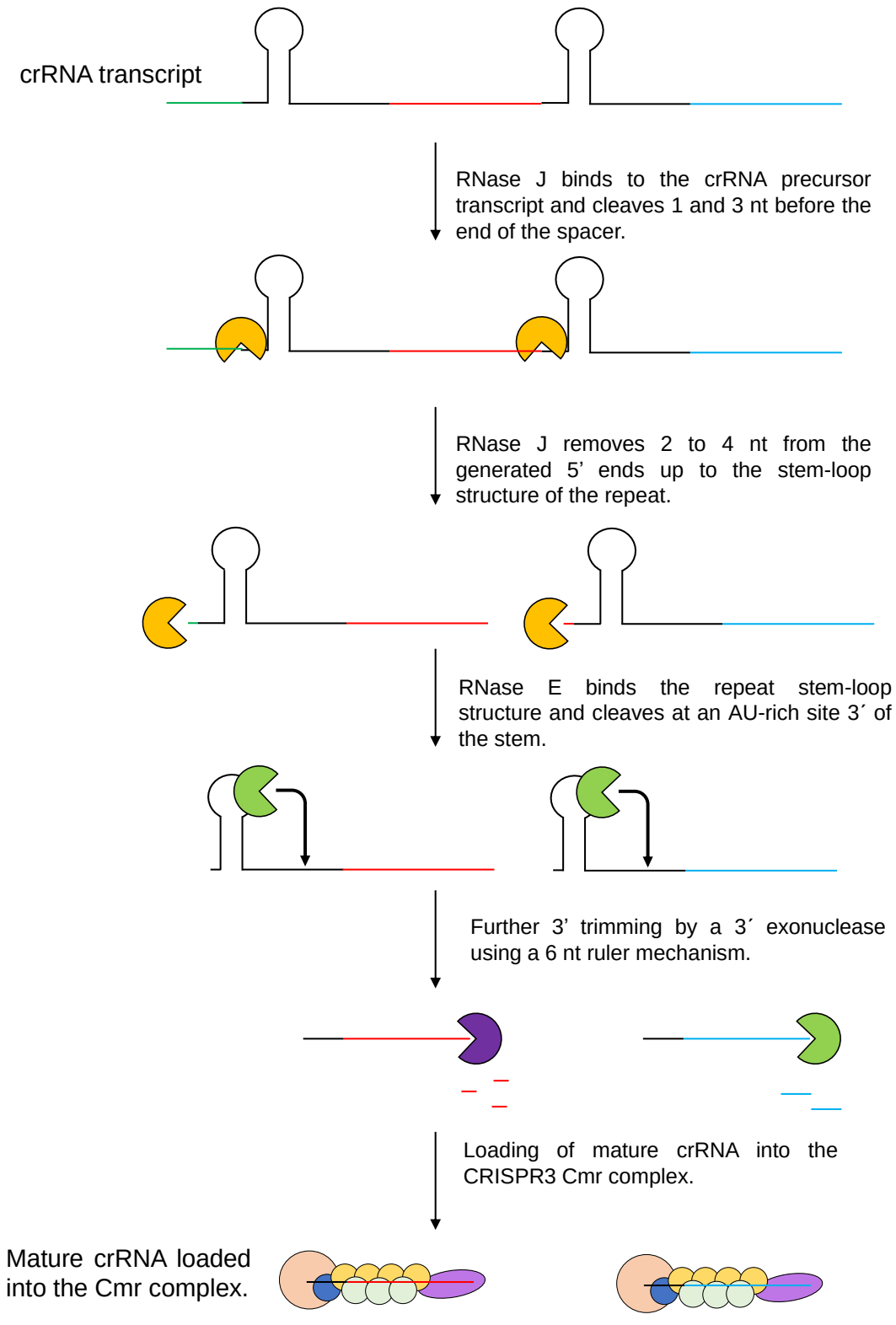

Figure 5. Model for the initiation of the maturation of CRISPR3-derived crRNAs. The transcribed CRISPR3 pre-crRNA (repeats in black) is recognized by RNase J (yellow) cleaving the transcript 1 and 3 nt from the spacer 3' end, described as the initial processing step (Scholz *et al.* 2013), followed by 5´end trimming by 2 to 4 nt until

reaching the stem-loop structure located at the beginning of the repeat sequence. RNase E (green) then recognizes the CRISPR repeat stem-loop structure and cleaves the RNA in the AU rich region downstream of the stem. This yields the mature 48 nt long crRNAs with a 13 or 14 nt 5´handle (Behler *et al.* 2018). Further 3´ trimming to the 42 nt mature crRNAs requires an unknown ribonuclease. As the PNPase (purple) interacts with both RNase E (Zhang *et al.* 2014) and RNase J (this study), this 3´-5´exoribonuclease may process the 3´ end of the crRNA to generate the 42 nt mature crRNAs. Both the 42 nt and 48 nt mature crRNA forms accumulate *in vivo* (Scholz *et al.* 2013). The mature crRNAs are then loaded into the CRISPR3-Cas protein complex.

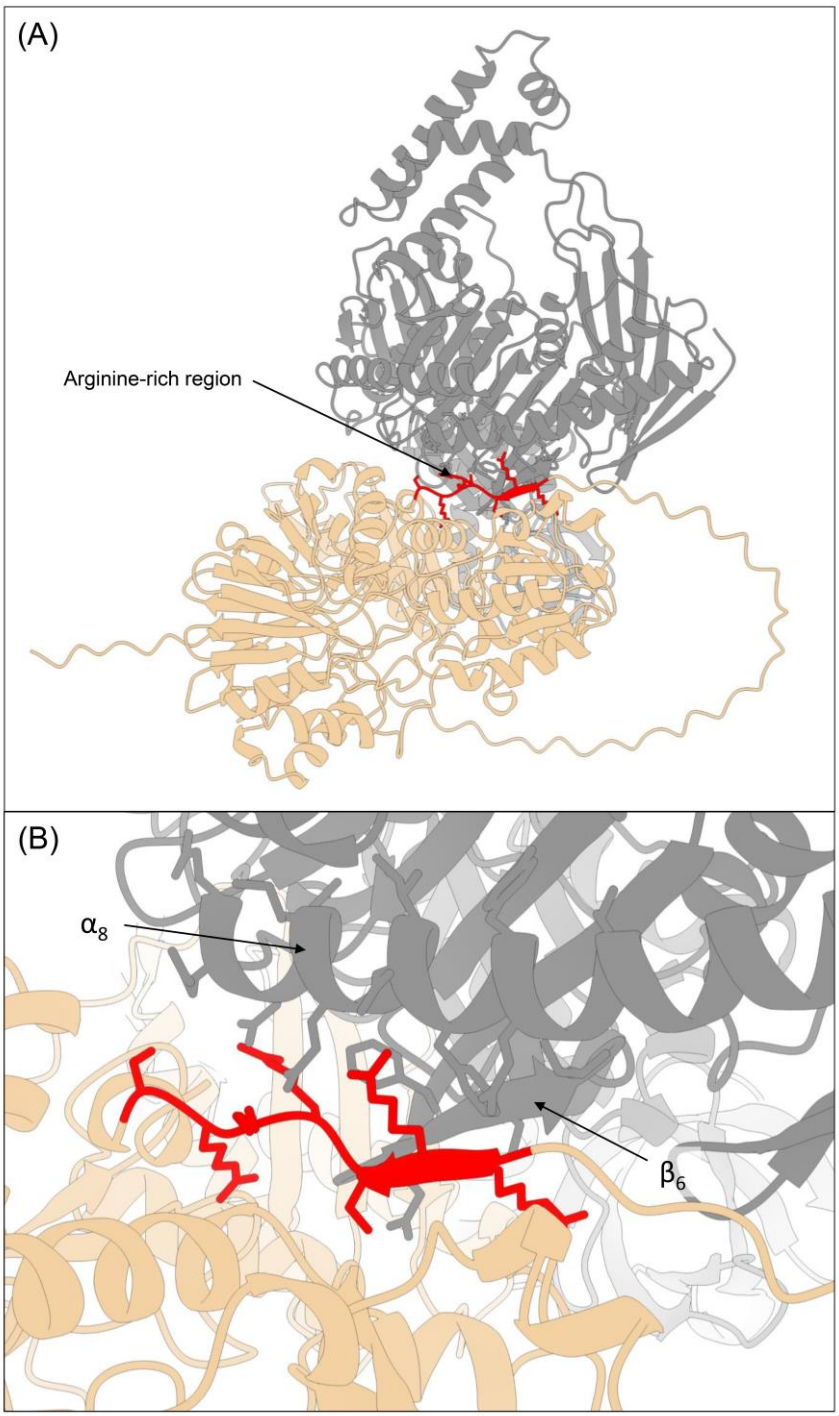

Figure 6. Predicted interaction of RNase J and PNPase. (A) Best-scoring structure of the RNase J-PNPase complex predicted by Alphafold 3 (pTM 0.52, iPTM 0.51). RNase J (light orange) has a small interaction surface with PNPase (gray). The arginine-rich motif at the CTD of RNase J is shown in red. **(B)** Enlargement of the interaction site. The arginine-rich motif of the CTD is in close proximity to a PNPase alpha helix (α_8, residues 196–208) and a β-sheet (β_6, residues 158–161).

Tables

Table 1. Protein class attribution of RNase J-coenriched proteins. The 27 and 36 proteins enriched in the co-IP with NTT, or CTT RNase J, respectively, were analyzed with PANTHER (Thomas *et al.* 2022) and classified according to their protein class category. Protein classes are shown in the middle. Percentage of protein class attributions identified in the NTT RNase J co-IP are shown in the left column, and those identified in the CTT co-IP in the right column.

NTT RNase J	Protein class	CTT RNase J
7.40%	transporter (PC00227)	14.30%
3.70%	gene-specific transcriptional regulator (PC00264)	2.90%
3.70%	translational protein (PC00263)	34.30%
11.10%	chaperone (PC00072)	5.70%
3.70%	protein-binding activity modulator (PC00095)	11.40%
25.90%	metabolite interconversion enzyme (PC00262)	2.90%
0%	DNA metabolism protein (PC00009)	8.60%
14.80%	protein modifying enzyme (PC00260)	5.70%
29.60%	unclassified	14.30%

Table 2. Proteins enriched in the co-IP with N-terminally tagged RNase J. Proteins identified in the 3×FLAG-RNase J co-IP and MS analysis passing the selection threshold ($log_2FC \geq 1.5$, p value ≤0.05). Shaded entries indicate proteins also found in the enrichment with C-terminally tagged RNase J. Results from the MS analysis are also plotted in **Fig. 3**.

R	log_2FC	Accession	Genes	ID	Description
1	10.26	RNJ_SYNY3	*rnj*	*slr0551*	ribonuclease J (bait)
2	5.39	P72746_SYNY3	*slr1102*	*slr1102*	c-di-GMP-related FHA-PAS-PAS-GGDEF-EAL protein (Enomoto, Wallner and Wilde 2023)
3	4.67	PNP_SYNY3	*pnp*	*sll1043*	polyribonucleotide nucleotidyltransferase
4	3.72	KPYK1_SYNY3	*pyk1*	*sll0587*	pyruvate kinase 1
5	2.78	Q55734_SYNY3	*sll0395*	*sll0395*	phosphoglycerate mutase (2,3-diphosphoglycerate-dependent)
6	2.31	Q55457_SYNY3	*ebsA*	*slr0038*	EbsA, essential for biofilm self-suppression, interacts with Hfq and PilB (Yegorov *et al.* 2021)
7	2.05	P72815_SYNY3	*sll1656*	*sll1656*	DUF3611
8	2.05	SYW_SYNY3	*trpS*	*slr1884*	tryptophan-tRNA ligase
9	1.93	P73800_SYNY3	*slr1260*	*slr1260*	DUF3122
10	1.91	PURT_SYNY3	*purT*	*slr0861*	phosphoribosylglycinamide formyltransferase
11	1.89	Q55448_SYNY3	*pisG*	*sll0038*	PatA family regulator of phototaxis (Yoshihara *et al.* 2000)
12	1.88	ARSA_SYNY3	*sll0086*	*sll0086*	one-domain ArsA-like protein
13	1.84	Q55780_SYNY3	*slr0208*	*slr0208*	peptidyl-prolyl cis-trans isomerase
14	1.79	P74157_SYNY3	*sll1384*	*sll1384*	DnaJ and TRP_11 domains
15	1.74	P73793_SYNY3	*sll1150*	*sll1150*	plasma membrane protein
16	1.73	RBCR_SYNY3	*rbcR*	*sll0998*	RuBisCO transcriptional regulator (Bolay *et al.* 2022)
17	1.70	P74275_SYNY3	*putA*	*sll1561*	delta-1-pyrroline-5-carboxylate dehydrogenase
18	1.67	P72756_SYNY3	*sll1033*	*sll1033*	protein-serine/threonine phosphatase
19	1.65	NTCA_SYNY3	*ntcA*	*sll1423*	global nitrogen regulator NtcA
20	1.65	HHOA_SYNY3	*hhoA*	*sll1679*	putative serine protease HhoA
21	1.65	KAD2_SYNY3	*adk2*	*sll1059*	adenylate kinase 2
22	1.62	CLPB1_SYNY3; CLPB2_SYNY3	*clpB1, clpB2*	*slr1641, slr0156*	chaperone ClpB 2
23	1.61	Q55514_SYNY3	*slr0552*	*slr0552*	gene located downstream of *rnj*
24	1.60	P73886_SYNY3	*ychF*	*sll0245*	ribosome-binding ATPase YchF

25	1.58	P73008_SYNY3	*mcpA*	*slr1044*	methyl-accepting chemotaxis protein
26	1.56	Y1654_SYNY3	*sll1654*	*sll1654*	universal stress protein
27	1.51	P72700_SYNY3	*slr0244*	*slr0244*	universal stress protein

Table 3. Proteins enriched in the co-IP with the C-terminally tagged RNase J. Proteins identified in the 3×FLAG-RNase J co-IP and MS analysis passing the selection threshold ($log_2FC \geq 1.5$, p value ≤ 0.05). Shaded entries indicate proteins also found in the enrichment with N-terminally tagged RNase J. Results from the MS analysis are also shown in **Fig. 3**.

R	log_2FC	Accession	Genes	ID	Description
1	12.13	RNJ_SYNY3	*rnj*	*slr0551*	ribonuclease J (bait)
2	5.96	PNP_SYNY3	*pnp*	*sll1043*	polyribonucleotide nucleotidyltransferase
3	4.28	Y1764_SYNY3	*slr1764*	*slr1764*	TerD domain (found in a stress response operon)
4	3.14	THIO2_SYNY3	*slr1139*	*slr1139*	thioredoxin-like protein
5	2.98	P73466_SYNY3	*sll1142*	*sll1142*	bifunctional nuclease domain
6	2.92	RRE1_SYNY3	*rre1*	*slr1783*	response regulator Rre1
7	2.68	P72756_SYNY3	*sll1033*	*sll1033*	protein-serine/threonine phosphatase
8	2.56	P73804_SYNY3	*aqpZ*	*sll1961*	GntR-family transcription factor
9	2.49	PUR7_SYNY3	*purC*	*slr1226*	phosphoribosylaminoimidazole-succinocarboxamide synthase
10	2.32	P74344_SYNY3	*moeB*	*sll1536*	molybdopterin biosynthesis protein MoeB
11	2.22	FTSZ_SYNY3	*ftsZ*	*sll1633*	cell division protein FtsZ
12	2.04	TRPA_SYNY3	*trpA*	*slr0966*	tryptophan synthase alpha chain
13	2.03	P72700_SYNY3	*slr0244*	*slr0244*	universal stress protein
14	2.01	P73886_SYNY3	*ychF*	*sll0245*	ribosome-binding ATPase YchF
15	1.97	IF2_SYNY3	*infB*	*slr0744*	translation initiation factor IF-2
16	1.96	P73497_SYNY3	*slr1240*	*slr1240*	unknown protein
17	1.94	GPX1_SYNY3	*gpx1*	*slr1171*	hydroperoxy fatty acid reductase Gpx1
18	1.89	Q55514_SYNY3	*slr0552*	*slr0552*	gene located downstream of *rnj*
19	1.85	DNAJ1_SYNY3	*dnaJ1*	*sll0897*	chaperone protein DnaJ 1
20	1.85	TOP1_SYNY3	*topA*	*slr2058*	DNA topoisomerase 1
21	1.80	Q55457_SYNY3	*ebsA*	*slr0038*	EbsA, essential for biofilm self-suppression, interacts with Hfq and PilB (Yegorov *et al.* 2021)
22	1.80	SSB2_SYNY3	*slr1034*	*slr1034*	thylakoid-associated single-stranded DNA-binding protein
23	1.79	Q55667_SYNY3	*slr0006*	*slr0006*	L-threonylcarbamoyl-adenylate synthase
24	1.76	RECA_SYNY3	*recA*	*sll0569*	protein RecA
25	1.71	IF3_SYNY3	*infC*	*slr0974*	translation initiation factor IF-3

26	1.70	Q55432_SYNY3	*sll0822*	*sll0822*	AbrB-like transcriptional regulator
27	1.69	P74756_SYNY3	*slr0609*	*slr0609*	CobW/HypB/UreG, nucleotide-binding domain
28	1.65	ARSA_SYNY3	*sll0086*	*sll0086*	one-domain ArsA-like protein
29	1.65	CLPB1_SYNY3; CLPB2_SYNY3	*clpB1, clpB2*	*slr1641 , slr0156*	chaperone protein ClpB 2
30	1.65	Q55822_SYNY3	*cobW*	*slr0502*	CobW protein
31	1.64	Q55448_SYNY3	*sll0038*	*sll0038*	PatA subfamily
32	1.59	THIO_SYNY3	*trxA*	*slr1139*	thioredoxin
33	1.56	Q55662_SYNY3	*clpC*	*sll0020*	ATP-dependent Clp protease regulatory subunit
34	1.51	OCP_SYNY3	*ocp*	*slr1963*	Orange carotenoid-binding protein
35	1.51	SSB1_SYNY3	*ssb*	*slr0925*	single-stranded DNA-binding protein 1
36	1.50	RBCR_SYNY3	*rbcR*	*sll0998*	RuBisCO transcriptional regulator (Bolay *et al.* 2022)